J. Fluid Mech. (1999), *vol.* 387, *pp.* 39–60. Printed in the United Kingdom

© 1999 Cambridge University Press

Direct numerical simulation of a puff and a slug in transitional cylindrical pipe flow

By H. SHAN[1], B. MA[1], Z. ZHANG[1] AND F. T. M. NIEUWSTADT[2]†

[1]Department of Engineering Mechanics, Tsinghua University, Beijing 100084, P.R. China

[2]J. M. Burgers Centre, Delft University of Technology, 2628 AL Delft, the Netherlands

(Received 11 June 1997 and in revised form 12 May 1998)

A direct numerical simulation of transitional pipe flow is carried out with the help of a spectral element method and used to investigate the localized regions of 'turbulent' flow that are observed in experiments. Two types of such regions can be distinguished: the puff and the slug. The puff, which is generally found at low values of the Reynolds numbers, is simulated for $Re = 2200$ where the Reynolds number Re is based on the mean velocity U_B and pipe diameter D. The slug occurs at a higher Reynolds number and it is simulated for $Re = 5000$. The computations start with a laminar pipe flow to which is added a prescribed velocity disturbance at a given axial position and for a finite time. The disturbance then evolves further into a puff or slug structure.

The simulations confirm the experimentally observed fact that for a puff the velocity near the leading edge changes more gradually than for a slug where an almost discontinuous change is observed. The positions of the leading and trailing edges of the puff and slug are computed from the simulations as a function of time. The propagation velocity of the leading edge is found to be constant and equal to $1.56U_B$ and $1.69U_B$ for the puff and slug, respectively. For the trailing edge the velocity is found to be $0.73U_B$ and $0.52U_B$, respectively. By rescaling the simulation results obtained at various times to a fixed length, we define an ensemble average. This method is used to compute the average characteristics of the puff and slug such as the spatial distribution of the mean velocity, the turbulent velocity fluctuations and also the wall shear stress. By computing particle trajectories we have investigated the entrainment and detrainment of fluid by a puff and slug. We find that the puff detrains through its trailing edge and entrains through its leading edge. The slug entrains fluid through its leading and through most of its trailing edge. As a consequence the fluid inside the puff is constantly exchanged with fluid outside whereas the fluid inside a slug remains there. These entrainment/detrainment properties which are in agreement with the measurements of Wygnanski & Champagne (1973) imply that the puff has the characteristics of a wave phenomenon while the slug can be characterized more as a material property which travels with the flow.

Finally, we have investigated in more detail the velocity field within the puff. In a coordinate system that travels with the mean velocity we find recirculation regions both near the trailing and leading edges which agrees at least qualitatively with experimental data. We also find streamwise vortices, predominantly in the trailing-edge region which have been also observed in experiments and which are believed to play an important role in the dynamics of the transition process.

† Author to whom correspondence should be addressed: e-mail f.nieuwstadt@wbmt.tudelft.nl.

https://doi.org/10.1017/S0022112099004681 Published online by Cambridge University Press

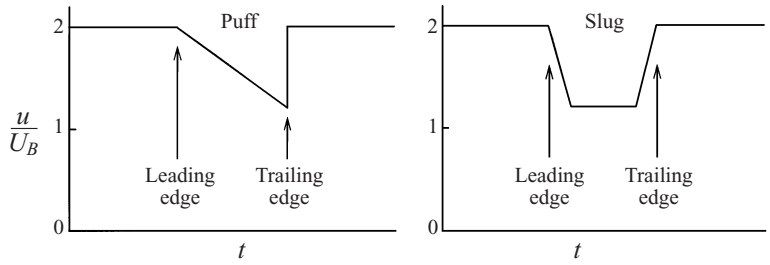


FIGURE 1. Schematic trace of the velocity of a puff and a slug as a function of time during their passage past a single observation point on the centreline of the pipe.

1. Introduction

The study of transition from laminar to turbulent flow in a cylindrical pipe started with the famous experiments of Reynolds (1883). He showed that transition depended on a non-dimensional number which since then has been named after him. For values of the Reynolds number smaller than about 2000 the flow was observed to stay laminar irrespective of any disturbance in the flow. However, another observation made by Reynolds was that the flow could be kept laminar for larger values than 2000 if flow disturbances were avoided. The smaller the disturbance the larger the Reynolds number to which laminar flow could be extended. With his own experimental setup Reynolds was able to reach a maximum Reynolds number up to 12 000. Since then it has been confirmed in a number of other experiments that by avoiding disturbances, a cylindrical pipe flow can be kept laminar until very large Reynolds numbers (see e.g. Draad 1996 for a review).

The transition process in pipe flow has been studied further in various other experimental investigations and in particular by Wygnanski and co-workers (Wygnanski & Champagne 1973; Wygnanski, Sokolov & Friedman 1975). They found that beyond the critical Reynolds number of 2000 flow disturbances evolve into localized regions of 'turbulence'. These regions, which fill the pipe cross-section, travel downstream with the flow and they can be compared with the well-known turbulent spot in a transitional boundary layer.

Wygnanski & Champagne (1973) also found that there are two types of these localized, turbulent-like structures: the puff and the slug. The puff is found when the Reynolds number is below $Re \sim 2700$ and the slug appears when the Reynolds number is above $Re \sim 3000$. Both the puff and the slug are characterized by a distinct trailing edge over which the flow changes almost discontinuously from the 'turbulent' flow conditions inside the structure to the laminar flow outside. The puff and slug are, however, different with respect to their leading edge. For the puff the change of velocity near the leading edge is rather gradual and it changes smoothly from the laminar velocity in front of the puff to the 'turbulent' velocity inside it. The change of velocity near the leading-edge of a slug is again quite sudden. A schematic picture of this behaviour of the centreline velocity which distinguishes the puff from the slug, is given in figure 1.

Various other experimental studies, e.g. those by Darbyshire & Mullin (1995), have also shown that the characteristics of a puff and slug are independent of the details of the initial disturbance from which they evolve. In addition, it was found that the puff and slug are also independent of the mean flow conditions, i.e. whether the pipe flow has a constant pressure drop or a constant flow rate.

https://doi.org/10.1017/S0022112099004681 Published online by Cambridge University Press

All these experiments have provided much data on the transition process in a pipe flow in general and on the related puff and slug structures in particular. Nevertheless, there is a need for more information, and in particular on the flow details, that can shed more light on the mechanism of the transition process because from a theoretical point of view the transition of cylindrical pipe flow is still an open problem. More detailed data could, therefore, inspire or assist theoretical progress.

Apart from laboratory experiments such information can at present be also obtained from numerical simulation. Such an approach has been applied with much success to the transition process of a boundary layer over a flat plate (see e.g. Kleiser & Zang 1991 for a review). Three-dimensional temporal simulations of transition in plane channel flows have been carried out by Orszag & Patera (1983). Some numerical results on the transition of a pipe flow were reported by O'Sullivan & Breuer (1994*a*, *b*) who have considered the role of transient growth.

In the present study we will also turn to a numerical investigation of transitional pipe flow. Different from the numerical studies mentioned above, our main objective is to perform a simulation of the puff and slug structure. To this end we perform a direct numerical simulation of a laminar pipe flow at a Reynolds number in which experimentally either a puff or slug has been found to develop. The puff or slug structure is triggered by imposing a localized velocity disturbance on the flow for a small period of time. After this excitation the disturbance is transported downstream and develops into either a puff or slug. From the computational results we are then able to study the full three-dimensional structure and characteristics of the puff and slug in detail.

The outline of this paper is as follows. First we consider the numerical techniques and computational procedures that we have used. Next we turn to a discussion of the simulation data in which we shall compare the results for the puff with those for the slug. Subsequently we will consider some details of the velocity field of the puff. We end with some conclusions.

2. Numerical techniques and computational procedures

The Navier–Stokes equations and the continuity equation for a Newtonian incompressible fluid flow expressed in vector notation read

$$\nabla \cdot \boldsymbol{v} = 0, \tag{2.1}$$

$$\frac{\partial \boldsymbol{v}}{\partial t} + \boldsymbol{\omega} \times \boldsymbol{v} = -\nabla P + \frac{2}{Re}\nabla^2 \boldsymbol{v} + \boldsymbol{f}, \tag{2.2}$$

where $\boldsymbol{v}$ is the velocity vector and $\boldsymbol{\omega} = \nabla \times \boldsymbol{v}$ the vorticity. P is defined as $P = p + |\boldsymbol{v}|^2/2$ with p the static pressure fluctuation; $\boldsymbol{f}$ is a forcing term taken to be $-(\mathrm{d}\bar{p}/\mathrm{d}x)\boldsymbol{e}_x$ with $\mathrm{d}\bar{p}/\mathrm{d}x$ the average pressure gradient in the streamwise direction. The equations have been non-dimensionalized by employing the pipe radius R as a characteristic length and bulk velocity U_B as a characteristic velocity. As a result, the Reynolds number $Re = U_B D/\nu$ appears in (2.2) in which ν is the kinematic viscosity and $D = 2R$ the pipe diameter.

A cylindrical coordinate system is most suited for the description of a pipe flow and therefore used in our study. Hereafter, r, θ and x will denote the radial, azimuthal and axial (streamwise) direction respectively, and w, v and u the radial, azimuthal and axial velocity.

To solve (2.1) and (2.2) numerically we use here a spectral method. The main advantage of such a method is its numerical accuracy which for an investigation

https://doi.org/10.1017/S0022112099004681 Published online by Cambridge University Press

of transition is essential. Application of spectral methods requires that our problem must satisfy some constraints such as periodicity. In the azimuthal direction the flow is periodic by definition. In our computation periodicity is also assumed in the axial direction over a length L. This implies the computed structures are limited in length by L. The assumption of periodicity in the axial direction is consistent with the fact that within the computational domain the flow is fully developed laminar outside the puff and slug. Other constraints to be satisfied are that in the radial direction, the velocity and total pressure are required to be single-valued at the centreline. On the pipe wall, the velocity should obey a no-slip condition.

With the periodic conditions in axial and azimuthal directions, a Fourier–Galerkin method is a natural choice. In the radial direction, a spectral element method is used by which the pipe can be subdivided into annular domains. We have chosen N_e such domains for which the radial coordinates of the outer boundaries are given by

$$r_j = (1 - r_c)\left\{\ln\left[\frac{N_e - j}{N_e - 1}(e - 1) + 1\right]\right\}^{1/2} + r_c, \tag{2.3}$$

where $j = 1, 2, \ldots N_e$ are the indices of the elements and r_c the radius of the central element. Inside each element, a Chebyshev-collocation method is used and the Gauss–Lobatto collocation points are defined in terms of a local coordinate $y \in [-1, 1]$ given by

$$y_k^j = \cos\frac{\pi k}{N_P^j},$$

where $k = 0, 1, 2, \ldots, N_P^j$ are the indices of collocation points. For the jth element, the expansions for the velocity and total pressure can then be written as

$$\boldsymbol{v}(y^j, \theta, x) = \sum_{m=-M/2}^{M/2-1} \sum_{n=-N/2}^{N/2-1} \sum_{k=0}^{N_P^j} \hat{\boldsymbol{v}}_k^j(m, n) h_k^j(y^j) \mathrm{e}^{\mathrm{i}(n\alpha x + m\theta)}, \tag{2.4}$$

$$P(y^j, \theta, x) = \sum_{m=-M/2}^{M/2-1} \sum_{n=-N/2}^{N/2-1} \sum_{k=0}^{N_P^j} \hat{P}_k^j(m, n) h_k^j(y^j) \mathrm{e}^{\mathrm{i}(n\alpha x + m\theta)}, \tag{2.5}$$

where h_k^j is the Lagrangian interpolation polynomial (Gottlieb, Hussaini & Orszag, 1984). On the interface of two adjacent elements, a C^1 continuity condition is used. In our computation we have taken $N_e = 4$ with $r_c = 0.1$ and in each element $N_P = 16$ except for the central element where $N_P = 4$.

To solve the time-dependent Navier–Stokes equations, we employ a time-splitting method with a third-order stiffly-stable scheme introduced by Karniadakis, Israeli & Orszag (1991). In this numerical scheme the nonlinear term, the pressure gradient term and the viscous term are integrated sequentially in the following three sub-steps:

$$\frac{\boldsymbol{v}^{n+1/3} - \sum_{q=0}^{2} \alpha_q \boldsymbol{v}^{n-q}}{\Delta t} = \sum_{q=0}^{2} \beta_q (\boldsymbol{v} \times \boldsymbol{\omega})^{n-q} - \boldsymbol{f}, \tag{2.6}$$

$$\frac{\boldsymbol{v}^{n+2/3} - \boldsymbol{v}^{n+1/3}}{\Delta t} = -\nabla P^{n+1}, \tag{2.7}$$

https://doi.org/10.1017/S0022112099004681 Published online by Cambridge University Press

$$\frac{\gamma_0 \boldsymbol{v}^{n+1} - \boldsymbol{v}^{n+2/3}}{\Delta t} = \frac{1}{Re}\nabla^2 \boldsymbol{v}^{n+1}, \tag{2.8}$$

where the superscript denotes the times step. The coefficients in (2.6) and (2.8) are given by $\alpha_0 = 3$, $\alpha_1 = -3/2$, $\alpha_2 = 1/3$, $\beta_0 = 3$, $\beta_1 = -3$, $\beta_2 = 1$ and $\gamma_0 = 11/6$.

The nonlinear term $\boldsymbol{v} \times \boldsymbol{\omega}$ in (2.6) is computed by means of a pseudo-spectral method and the aliasing error is removed by the 2/3 rule. With help of the continuity equation (2.1), (2.7) is transformed into a Poisson equation for the total pressure which is solved with use of the pressure boundary condition proposed by Karniadakis *et al.* (1991). The advantage of this pressure boundary condition is its efficient removal of time-splitting errors. The time-splitting errors are removed further by applying the Green's function correction proposed by Marcus (1984). The value of the forcing $\boldsymbol{f}$ is adjusted at every time step to ensure a constant bulk velocity U_B.

The code has been extensively tested for its stability properties. The only numerical instability found was the linear convective instability which can be avoided by setting the time step sufficiently small according the Courant–Friedrichs–Lewy (CFL) criterion.

Furthermore, the code has been validated by the following three test cases. In the first case, a standard parabolic profile of the axial velocity was computed starting from an initially zero-velocity field by imposing a fixed streamwise pressure gradient. In the second case, a linear distribution of the azimuthal velocity in the radial direction is attained by starting from a zero-velocity field in a pipe rotating around its axis at a constant angular velocity. In the third case we considered a small axisymmetric disturbance with streamwise wavelength of $\alpha = 6.2$ at a Reynolds number $Re = 500$. Linear stability theory predicts that this disturbance decays according to

$$E(t) = E(0)\mathrm{e}^{2\omega_i t}$$

where $E(t)$ is the energy of the disturbance. From linear stability theory we find $\omega_i = -0.39184$. The value obtained from the computation with our code is $\omega_i = -0.39188$. Based on these tests we trust our numerical code to produce correct results.

The puff and slug are triggered by exciting the initial laminar Poiseuille profile with a disturbance. This disturbance is imposed in the form of local blowing and suction of fluid through a slit in the pipe wall. In our simulation this is enforced by prescribing the radial velocity at the pipe wall according to the expression

$$w_{\mathrm{dist}} = \frac{A_w(t)}{2}\left[\cos\frac{2\pi}{\Delta x}(x - x_c) + 1\right]\sin\theta \sin \Omega t, \tag{2.9}$$

where Ω denotes the disturbance frequency which is set equal to 8.45 in our computations. The x in (2.9) lies in the interval

$$x \in [x_c - \Delta x/2, x_c + \Delta x/2],$$

where x_c indicates the centre of the perturbation region and Δx the width of the region. For the case of the puff the values of both x_c and Δx have been taken equal to π and for the slug $x_c = 8\pi$ and $\Delta x = 0.75\pi$. The amplitude envelope function $A_w(t)$ is illustrated in figure 2. In our case, $T_i = 1.0$, $T_d = 2.0$, $T_e = 0.5$ and the maximum of $A_w(t)$ is set equal to 1.1 which implies that the suction/blowing velocity is of the same order of magnitude as the bulk velocity.

Further computational details for our puff and slug computations are collected in table 1.

The computations have been carried out on the Cray-C90 of the academic computing centre SARA in Amsterdam. For the slug flow with the number of grid points

https://doi.org/10.1017/S0022112099004681 Published online by Cambridge University Press

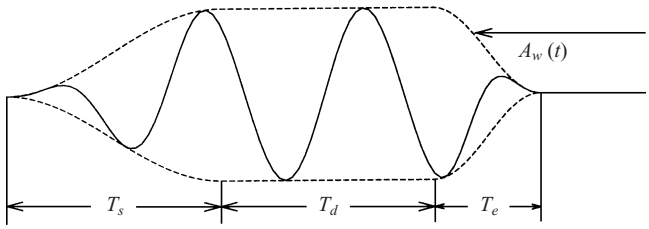


FIGURE 2. Shape of the velocity disturbance used to trigger the puff and slug as function of time.

	Puff	Slug
Re	2200	5000
N_x	128	256
N_θ	16	64
N_r	53	53
Δt	0.000929	0.0005
L	32π	32π

TABLE 1. Computational details for the puff and slug computation: Re is the Reynolds number based on the mean velocity and pipe diameter; N_x, N_θ and N_r are the number of collocation points in the axial, tangential and radial direction; Δt is the time step in the numerical computations non-dimensionalized with U_B and the pipe radius R; L is the pipe length non-dimensionalized with the radius R.

given in table 1, one time step takes 18 CPU s. For the total simulation we used 40 000 time steps which thus amounts to 200 CPU hours. The number of grid points is approximately the same as used by Eggels *et al.* (1994) for the computation of a fully developed pipe flow at $Re = 5000$. However, Eggels *et al.* (1994) took the length of the computational domain to be $10R$ whereas in our case it is $32\pi R$. This difference is the consequence of a compromise that we had to make in view of our aim to compute the downstream development of the puff and slug structure and the need to resolve all flow details. It means that the resolution in the axial direction may be considered as not optimal at least for a completely resolved simulation of a fully developed turbulent flow. However, we expect the instability processes which determine the puff and slug structure to be mainly influenced by the large flow scales which are believed to be adequately resolved by our computation.

3. Comparison of the puff and slug structure

The selection of the Reynolds numbers for the puff and slug computation was based on the following criteria. From experiments (e.g. Wygnanski & Champagne 1973) it is known that puffs appear when $Re \lesssim 2700$ and slugs for $Re \gtrsim 3000$. Furthermore, Wygnanski *et al.* (1975) claim to observe for $Re \simeq 2200$ a so-called equilibrium puff. This is a puff which travels down the pipe without changing its size. We have selected this Reynolds number because an equilibrium puff would have made our averaging procedure to be discussed below more convenient. The puff in our computations at $Re = 2200$ does not satisfy the characteristic of an equilibrium puff that it stays constant in size. The reason is probably that our computational domain is too short for the equilibrium to become established but

https://doi.org/10.1017/S0022112099004681 Published online by Cambridge University Press

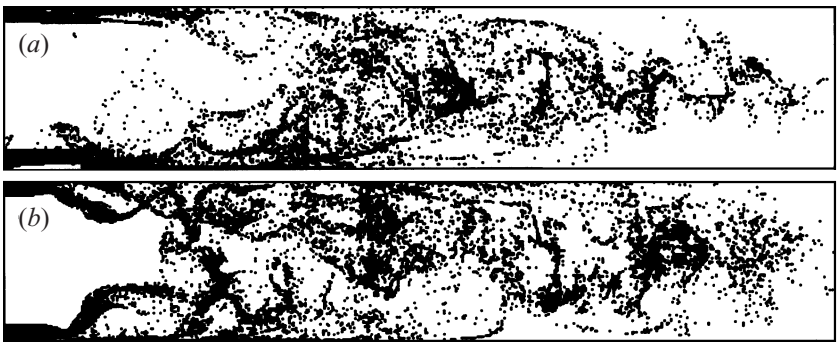


FIGURE 3. Numerical flow visualization of the instantaneous structure of (*a*) a puff at $t = 60$; (*b*) a slug at $t = 50$.

it should be also mentioned that it is far accepted whether such equilibrium puff indeed exists. The Reynolds number for the slug was selected because at about the same Reynolds number we have the results available of a direct numerical simulation of fully developed pipe flow (Eggels *et al.* 1994). Thus we are able to compare the velocity statistics of a slug with those of fully developed turbulent pipe flow.

Both the puff and the slug are generated by the local blowing/suction method discussed in the previous section. After the end of the disturbance period, the flow disturbance develops further under the influence of its own dynamics. This means that it is transported by the velocity down the pipe while at the same time it grows in size. When the leading edge of the disturbance reaches the end of the pipe, the periodic boundary conditions that we use cause the disturbance to re-enter the beginning of the pipe. As a result we can follow the development of the disturbance and the resulting puff or slug structure until the leading edge comes too close to the trailing edge. When this happens the computation has to be stopped.

Before we start to analyse the numerical data by quantitative methods, we first show a qualitative visualization of our numerical results. This 'numerical visualization' is shown in figure 3. To obtain it we introduce in the flow a passive dye in the form of marked fluid particles starting at given time and at a fixed x-position which is just downstream of the leading edge of the structure at that time. The dye is emitted near the pipe wall from two opposite points. When the structure passes the emission location, the dye is entrained into the puff or slug and is carried along while tracing the structure. This procedure resembles the method used by Bandyopadhay (1986) in his experimental visualization of an equilibrium puff. The instantaneous distribution of the tracer is shown in figure 3 for $t = 60$ and $t = 50$ for the puff and slug, respectively.

The figure shows the main characteristics of the puff and slug structure. Wave-like motions are visible which have been also observed in experiments. In particular we observe in the near-wall region upstream of the trailing edge of the puff some vortex-like structures which were also noted by Bandyopadhay (1986). In addition, the figure shows that near the leading edge the puff and slug have a quite different structure which agrees with our schematic picture of both structures shown in figure 1. On comparing these 'numerical visualizations' with the experimental visualization of Bandyopadhay (1986), we tend to conclude that our simulated structures exhibit quite realistic features.

https://doi.org/10.1017/S0022112099004681 Published online by Cambridge University Press

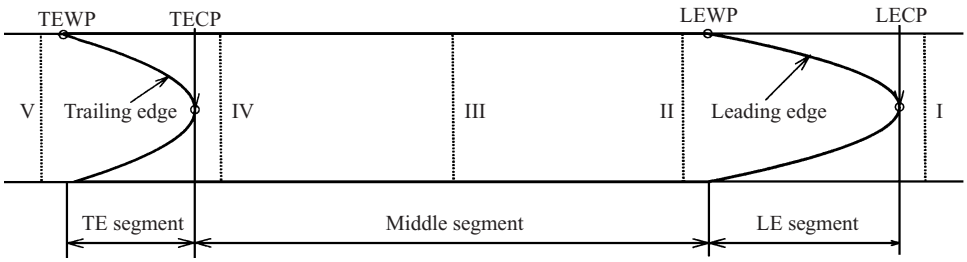


FIGURE 4. Definition of the various puff/slug elements and the location of the characteristic points: leading-edge centreline point (LECP), leading-edge wall point (LEWP), trailing-edge centreline point (TECP), trailing-edge wall point (TEWP); the planes indicated by the numerals I–V are used as starting positions for the release of particles.

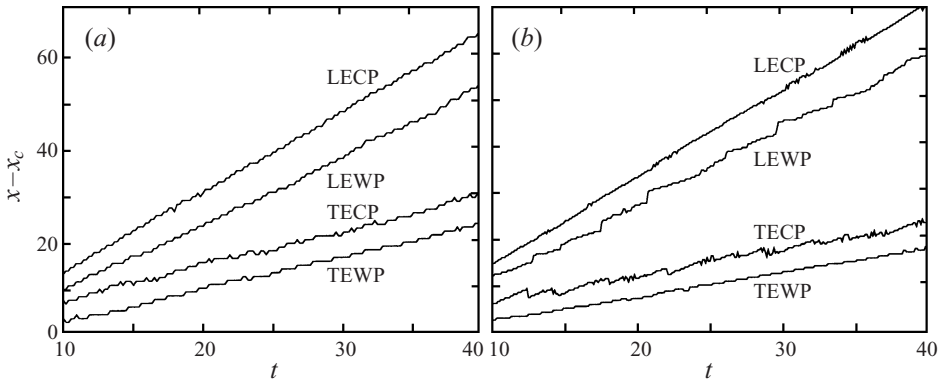


FIGURE 5. Position of LECP, LEWP, TECP and TEWP as a function of time: (*a*) puff; (*b*) slug.

3.1. *Puff and slug growth and their propagation velocity*

Both the puff and the slug grow in size when they are moving down the pipe. This development can be studied by plotting the position of some characteristic points of the puff/slug as a function of time.

These characteristic points are defined here as the intersection of the leading and trailing edge of the structure with the pipe centreline and with the wall, as illustrated in figure 4. The following procedure is used to locate these points in our simulation results. For each time we compute the root-mean-square (r.m.s.) of the axial velocity fluctuations, $\langle u \rangle_{\mathrm{rms}}$, by taking an average over the azimuthal coordinate. Next the contour line of $\langle u \rangle_{\mathrm{rms}} = 10\% U_B$ is plotted. The foremost points on the leading and trailing edge of this contour line are defined as the leading-edge centre point (LECP) and trailing-edge centre point (TECP), respectively. The intersections of the line $r = 0.95R$ with the leading and trailing edge of the contour line are defined as the leading-edge wall point (LEWP) and trailing-edge wall point (TEWP). The region between the LECP and the LEWP is called the leading-edge segment and the region between the TECP and the TEWP the trailing-edge segment. The centre region is denoted the middle segment.

In figure 5 the positions of characteristic points introduced above are shown as a function of time. First, we would like to draw attention to the fact that the lines for the LECP are almost parallel to the lines for the LEWP, and similarly for the TECP

https://doi.org/10.1017/S0022112099004681 Published online by Cambridge University Press

	Puff	Slug
C_{LECP}	1.68 $\pm$ 0.015	1.81 $\pm$ 0.033
C_{LEWP}	1.44 $\pm$ 0.024	1.56 $\pm$ 0.063
C_{TECP}	0.74 $\pm$ 0.027	0.53 $\pm$ 0.052
C_{TEWP}	0.71 $\pm$ 0.025	0.50 $\pm$ 0.019

TABLE 2. Values of the coefficients which denote the velocity of the leading-edge and trailing-edge points.

and TEWP. This means that the leading-edge and trailing-edge segments (see figure 4) stay nearly constant as a function of time. This gives, in our opinion, some support to the subdivision of the puff/slug into the three separate segments we have discussed above. The size of the trailing-edge segment for the puff seems to be about equal to $\sim 10R$ which is reasonably close to the value of $3D$–$4D$ quoted by Bandyopadhay (1986).

We see in figure 5 that all characteristic points trace out an almost straight line as a function of time or in other words their convective speed is constant. These speeds are obtained by fitting a linear curve to the lines of figure 5 and the results are given in table 2.

Let us define the velocity of the leading edge and trailing edge as

$$U_{\mathrm{LE}} = C_{\mathrm{LE}} U_B, \tag{3.1}$$

$$U_{\mathrm{TE}} = C_{\mathrm{TE}} U_B, \tag{3.2}$$

with $C_{\mathrm{LE}} = \frac{1}{2}(C_{\mathrm{LECP}} + C_{\mathrm{LEWP}})$ and $C_{\mathrm{TE}} = \frac{1}{2}(C_{\mathrm{TECP}} + C_{\mathrm{TEWP}})$. Based on the results given in table 2 we find $C_{\mathrm{LE}} = 1.56$ and $C_{\mathrm{TE}} = 0.73$ for the puff and $C_{\mathrm{LE}} = 1.69$ and $C_{\mathrm{TE}} = 0.52$ for the slug.

For the case of the puff, Champagne & Wygnanski (1973) report for the convective speed of the leading edge a value equal to $0.92\,U_B$ and for the trailing edge $0.86\,U_B$. This result was obtained at $505\,x/D$ downstream from the pipe entrance where the perturbation was introduced. In the experiment carried out by Teitgen (1980) in a fully developed pipe flow at various Reynolds numbers, he finds at $Re = 2200$, $C_{\mathrm{LE}} = 1.40$ and $C_{\mathrm{TE}} = 0.73$ at $x/D = 300$ downstream of the perturbation. Considering the differences between these experimental values, we have no reason to reject our results for the puff given in table 2.

For the slug at $Re = 5000$ the data of Champagne & Wygnanski (1973) lead to 1.55 and 0.62 for the C_{LE} and C_{TE}, respectively. In a more recent experiment by Draad & Westerweel (1996) values of ~ 1.7 and ~ 0.6 were found for C_{LE} and C_{TE} for an artificially generated slug at $Re = 5800$ and at a distance $x/D = 9$–40 from the point where the disturbance was introduced. The latter results, for which the conditions are close to our case, agree particularly well with our computational data. However, in view of the discussion at the end of § 2, we cannot rule out that the computed values are in this case also influenced by insufficient numerical resolution.

Next we define the propagation speed C_P of the puff and slug down the pipe as the average of the leading-edge and trailing-edge speeds. Based on the results discussed above for C_{LE} and C_{TE}, we find $C_P = 1.1U_B$ for both the puff and slug which implies that both structures are transported with approximately the mean flow speed and thus can be interpreted as material properties of the flow.

https://doi.org/10.1017/S0022112099004681 Published online by Cambridge University Press

3.2. *Definition of the averaging procedure*

The continuous increase in size of the puff/slug complicates the taking of averages. In principle one could perform a real ensemble average, i.e. perform at each downstream position an average over many realizations of a puff/slug generated under the same conditions. However, such a procedure is clearly not feasible because the generation of a sufficiently large ensemble would take an impracticably large amount of computing time.

To construct an averaging procedure which can be used in our case, we assume that the structure of each puff/slug segment (see figure 4) is self-similar with respect to its instantaneous length during the time periods $20 < t < 50$ and $30 < t < 40$ for the puff and slug, respectively and over which we have collected the data for these structures. We now scale the structure observed at each time to a prescribed length. For this we shall distinguish between the leading-edge and trailing-edge segments on the one hand and the middle segment of both the puff and slug on the other hand (see figure 4). We choose here to scale both the leading-edge and trailing-edge segments to a length of one unit and the middle segment of the puff/slug to a length of two units. In the following we shall indicate the scaled coordinates by an asterisk, e.g. x^*.

After rescaling, puffs and slugs observed at different times will all have the same size. At each position x^* in this scaled coordinate system we can now define a time average. As mentioned above this procedure is in principle only justified if the puff and slug structure is self-similar. However, even if self-similarity is satisfied with respect to some average length of the puff/slug , the instantaneous length which we use here as scaling parameter will undoubtedly fluctuate around this average length. As a result we expect that our averaging procedure will introduce some smoothing of the puff and slug structure.

The time average in the rescaled coordinates defined above allows us to study the structure of a puff/slug as a function of the axial, radial and tangential coordinates. Apart from this time average we shall in general also average over all azimuthal positions at a fixed value of x^*. For the puff structure we also average over five realizations of the puff which are discussed in § 3.6. The results obtained with the procedure discussed above will be called ensemble averages in the following. We note here that this definition is close to what has been used by Wygnanski & Champagne (1973) and by Wygnanski *et al.* (1975). Turbulent fluctuations will be defined as the deviation of a value observed at a specific x^* location and time with respect to the ensemble average.

In the following sections we shall present some ensemble average statistics of the puff and slug structure.

3.3. *Axial velocity*

The ensemble average of the axial velocity has been computed in the rescaled coordinate system for various fixed values of the radial coordinate r. The results for the puff and slug are shown in figure 6.

Let us consider some of the characteristic features of the axial velocity profile of the puff and slug that can be observed in this figure. The velocity profile at the centreline, i.e. $r = 0$, should in principle show the behaviour which we have schematically illustrated in figure 1. Indeed we find that near the leading edge of a puff the velocity varies more gradually than for the slug. However, one should remember that we are showing here the velocity in rescaled coordinates for which the leading-edge segment of both the puff and slug have been scaled onto a unit length. This transformation may somewhat obscure the behaviour of the velocity as function

https://doi.org/10.1017/S0022112099004681 Published online by Cambridge University Press

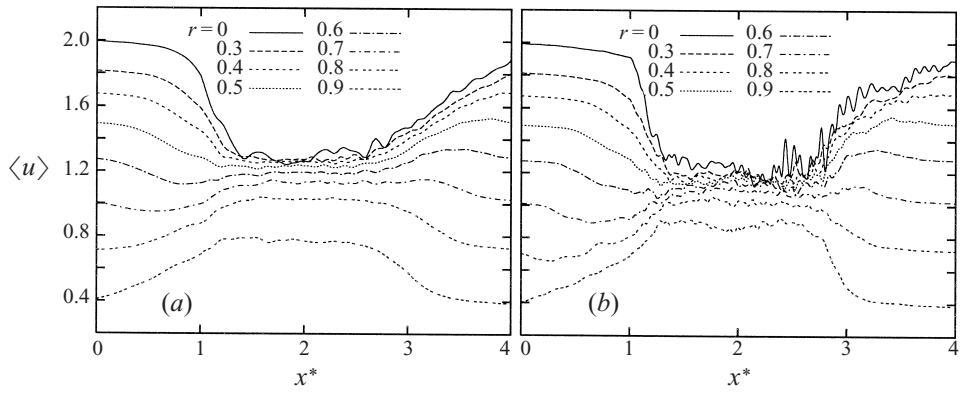


FIGURE 6. Ensemble-averaged axial velocity at fixed values of the radial coordinate r: (*a*) puff; (*b*) slug.

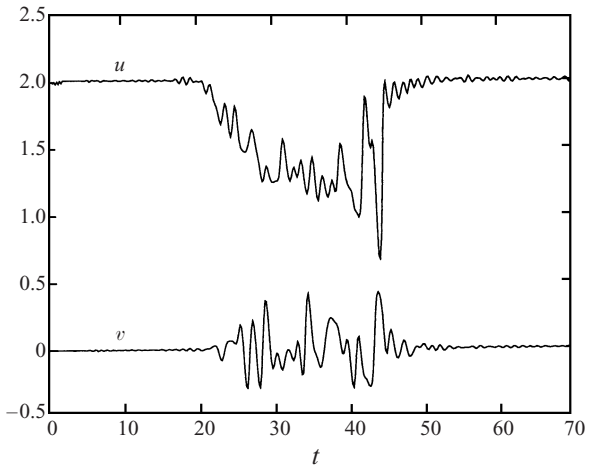


FIGURE 7. Time trace of the instantaneous axial and radial velocity at a fixed point on the centreline of the pipe.

of the real coordinate x but when plotting the instantaneous centreline velocity of the puff, we observe close agreement with figure 1. As a matter of fact the computational results shown in figure 7 are strikingly similar to experimental velocity traces obtained by Darbyshire & Mullin (1995).

From figure 6 it is also apparent that within the puff and slug the profile is more 'well-mixed' than the laminar profile. This agrees with the 'turbulent' character of the flow in both structures. Moreover, the 'well-mixedness' is larger for the slug than for the puff which would make the slug more turbulent than the puff.

Finally, we have plotted the mean velocity profiles as a function of r in figure 8. An inflection point appears in these profiles in the trailing-edge segment. These inflection points have been also observed in the experiments of Wygnanski & Champagne (1973). We shall come back to this result in § 4.

3.4. *Wall shear stress*

In figure 9 we show the ensemble-averaged wall shear stress in the rescaled coordinates for a puff and slug. We note that all variables shown, are non-dimensional. Therefore

https://doi.org/10.1017/S0022112099004681 Published online by Cambridge University Press

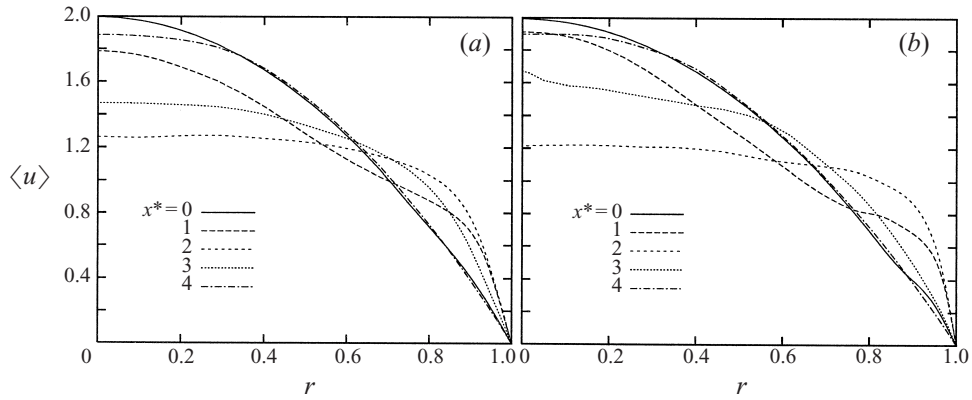


FIGURE 8. Ensemble-averaged axial velocity profiles at different rescaled coordinate x^*: (*a*) puff; (*b*) slug.

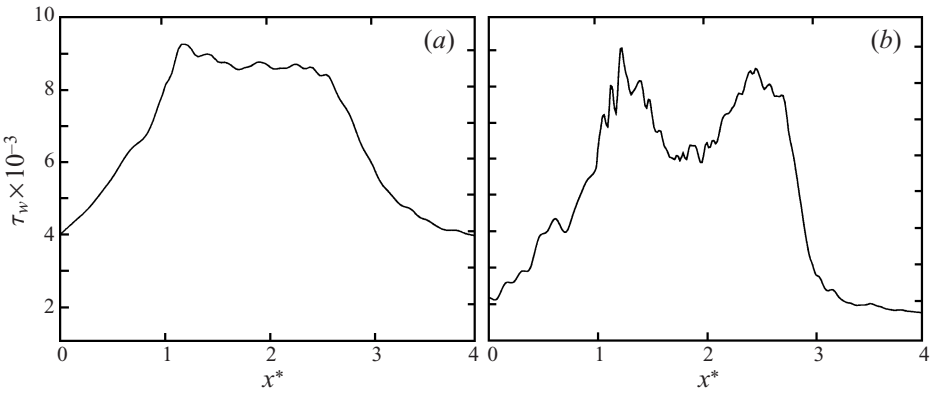


FIGURE 9. Ensemble average of the non-dimensional wall shear stress of the as a function of the rescaled coordinate x^*: (*a*) puff; (*b*) slug.

τ_w can be interpreted as $c_f/2$ where c_f is the local friction coefficient. We find that for both the puff and slug the maximum value of $\tau_w \simeq 0.009$. However the shape of the τ_w-profile is clearly different for the puff and slug. In the puff the value of the shear stress is approximately constant in the middle segment, while in the slug two maxima can be distinguished near both the leading and trailing edge. As a result the shear stress near $x^* = 2$, i.e. in the centre of the middle segment, is smaller for a slug than for a puff.

3.5. *Velocity fluctuations*

The velocity fluctuations have been computed according to the procedure mentioned in § 3.2. Based on the results we can compute the ensemble-averaged variance of these fluctuations as a function of the non-dimensional coordinates r and x^*. In figure 10 we show the isoline plots of the $u'u'$, $v'v'$ and $w'w'$ variances for both the puff and slug, respectively.

For the puff we observe a plateau of these variances in the middle segment. This is in agreement with the behaviour of the wall shear stress in this region shown in figure 9. In the slug all three variances exhibit local maxima which are located near the leading edge and trailing edge. This is also in agreement with the double maximum

https://doi.org/10.1017/S0022112099004681 Published online by Cambridge University Press

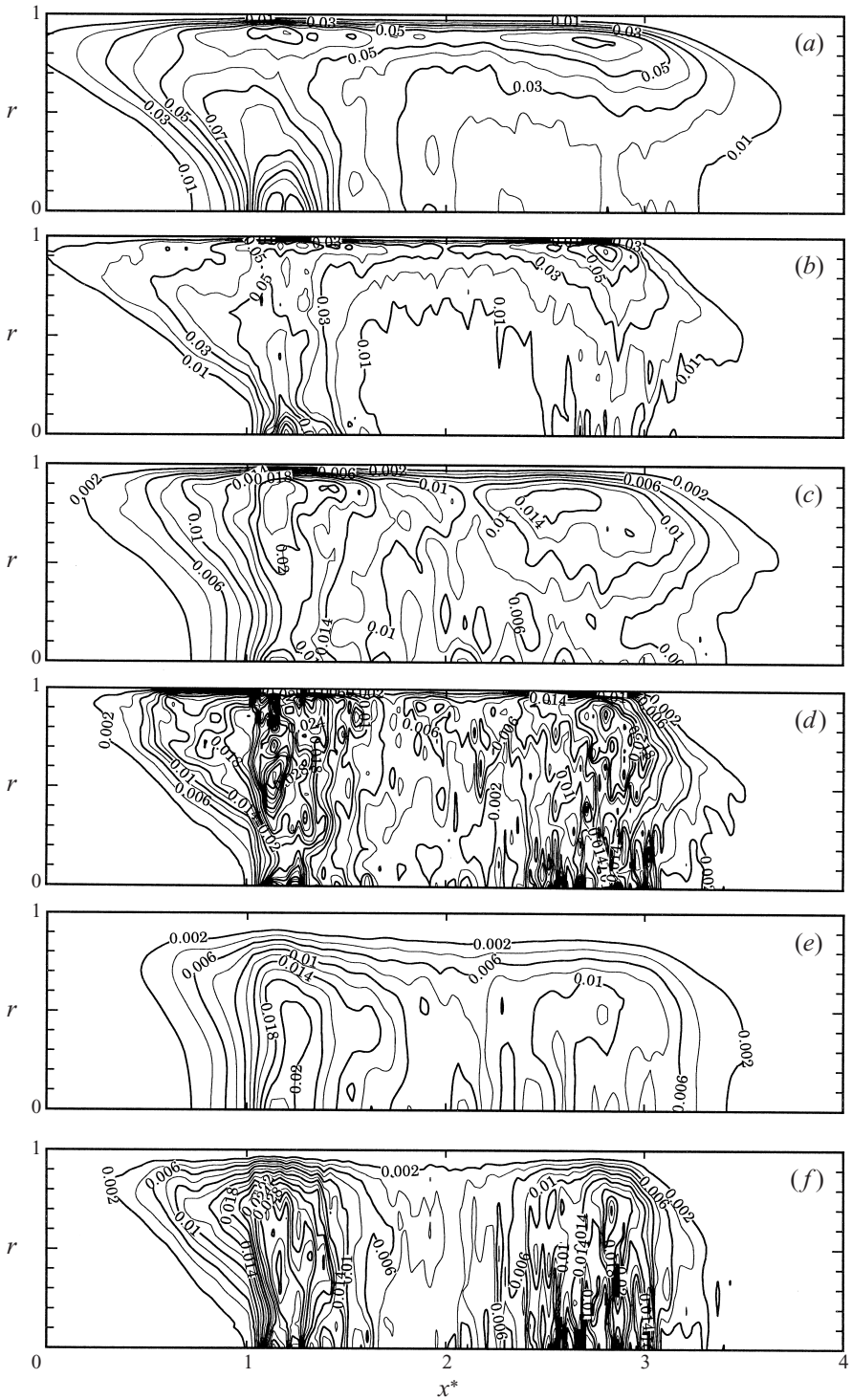


FIGURE 10. Isoline plot of the ensemble-averaged variances of velocity fluctuations: (*a*) (*c*) (*e*) puff $u'u'$, $v'v'$, $w'w'$; (*b*) (*d*) (*f*) slug $u'u'$, $v'v'$, $w'w'$.

https://doi.org/10.1017/S0022112099004681 Published online by Cambridge University Press

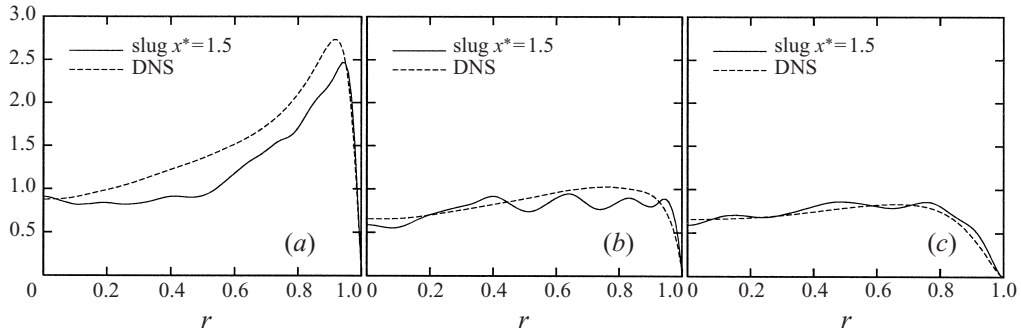


FIGURE 11. Radial distribution of the root mean square values (r.m.s.) of the axial $u_{\rm rms}$, azimuthal $v_{\rm rms}$ and radial $w_{\rm rms}$ velocity fluctuations at $x^* = 1.5$ in comparison with the r.m.s.-values obtained from a DNS of fully developed pipe flow at $Re = 5300$ (Eggels *et al.* 1994): (*a*) $u_{\rm rms}$; (*b*) $v_{\rm rms}$; (*c*) $w_{\rm rms}$

found in figure 9 for the wall shear stress. Moreover, the spatial distribution and also the value of the velocity variances in these regions are in reasonable agreement with experimental data, e.g. those of Wygnanski & Champagne (1973) and Wygnanski *et al.* (1975).

One may wonder whether the turbulence structure in the middle segment resembles that of a fully developed turbulent flow. To investigate this we consider for the slug the r.m.s. values of the axial, azimuthal and radial velocity fluctuations in the middle segment at $x^* = 1.5$. The results non-dimensionalized with the u_τ value obtained from the shear stress at the same x^* position, are given in figure 11. In the same figure we also show the r.m.s. values obtained from a DNS of fully developed pipe flow at $Re = 5300$ (Eggels *et al.* 1994) which is close to the Reynolds number of our slug simulation.

The r.m.s. profiles of the slug flow are found to be very close to the direct numerical simulation data for fully developed pipe flow. This result agrees with the observations of Wygnanski & Champagne (1973) who observe a close agreement between the turbulence inside the slug and that in fully developed pipe flow.

We note that this agreement can also be used as additional confirmation that our numerical resolution is adequate, perhaps with the axial direction as an exception where our slug data are found to be smaller than the fully developed turbulence profile. This seems consistent with the fact that in the axial direction our resolution differs very much from the resolution used by Eggels *et al.* (1994).

3.6. *Effect of initial perturbation*

It has been argued by several authors to whom we have referred in our introduction that the structure of the puff and slug is independent of the details of their initial conditions. To investigate whether our simulation can confirm this, we have computed the development of the puff for four additional initial conditions which have been constructed by adding a horizontal component to the wall-normal perturbation velocity given in (3.3) below. The magnitude of this horizontal velocity component has been taken to be 1% of the wall-normal velocity where the amplitude of the wall-normal velocity has been decreased so that the total disturbance energy remains constant.

In figure 12 we show the time evolution of the disturbance energy E_{dis} for the five

https://doi.org/10.1017/S0022112099004681 Published online by Cambridge University Press

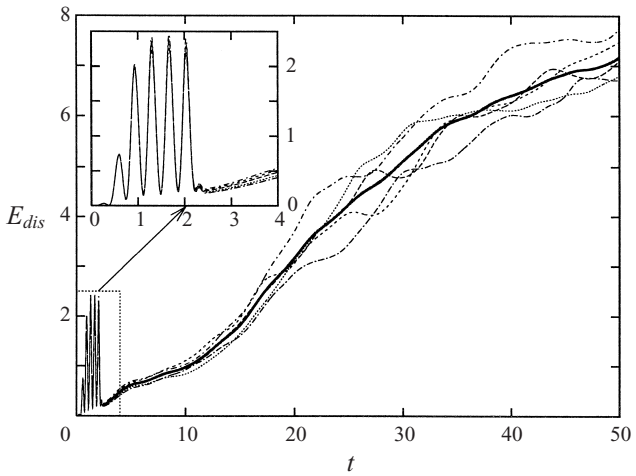


FIGURE 12. The disturbance energy E_{dis} of the puff as a function of time for the five computations with different initial conditions; the thick solid line represents the average over the five realizations.

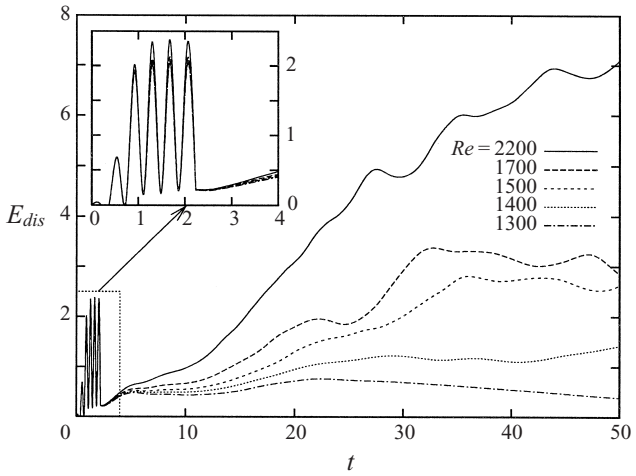


FIGURE 13. The disturbance energy E_{dis} of the puff as a function of time for the various values of the Reynolds number indicated in the figure.

initial conditions. Here, the disturbance energy is defined as

$$E_{dis} = \frac{1}{2}\int_0^1 \int_0^{2\pi} \int_0^{32\pi} (\boldsymbol{u} - \boldsymbol{u}_{\mathrm{lam}})^2 \, r \, \mathrm{d}r \, \mathrm{d}\theta \, \mathrm{d}x \tag{3.3}$$

which become identical to zero for laminar flow. The differences between the five realizations of the puff seem to be small which leads to the conclusion that the effects of initial conditions are indeed negligible. In the figure we also show by means of a thick solid line the average over the five realizations. This average has been used in all results for the puff that we have discussed and shown in this paper.

We have also performed computations of the puff for different values of the Reynolds number. The results for the disturbance energy as a function of time are illustrated in figure 13. We find that the growth of the disturbance energy decreases when the Reynolds number becomes smaller. Moreover, we find that for Reynolds

https://doi.org/10.1017/S0022112099004681 Published online by Cambridge University Press

numbers below 2200 the disturbance energy seems to reach a maximum value and decreases thereafter. This implies that the laminar flow in these cases can be considered as stable.

3.7. *Particle motion within a puff and slug*

To investigate the flow field within a puff and slug from a Lagrangian point of view, we have computed trajectories of fluid particles. The particles are released from several cross-sections which are shown in figure 4 numbered I to V. Note that these planes indicate the particle position at release time, i.e. $t = 20$ and $t = 30$ for the puff and slug, respectively.

The number of particles released is 900 and their initial position is randomly distributed over each plane. The trajectory of each particle is then computed with help of the instantaneous velocity fields which have been stored at time intervals $\delta t = 0.1$ which is about equal to 100 time steps for the puff and 200 time steps for the slug computation. This means that the influence on the trajectories of velocity variations on a time scale < 0.1 is ignored. This time scale is estimated to be smaller than the Kolmogorov time scale for fully developed turbulence at both Reynolds numbers. Therefore, the error due to the finite time step is estimated to be small. For the numerical procedure we use a simple explicit first-order Euler scheme for which the velocity at each particle location is determined from the stored velocity fields by means of linear interpolation. We have checked that this procedure is sufficiently accurate for the computation of particle statistics by performing a computation with a more accurate spectral interpolation method.

In figure 14 we show the positions of the particles released from the five cross-sections as a function of time in the form of line histograms. The length of the histogram denotes the range in particle position and the width is proportional to the number of particles that are present at the given location. We also show with a dashed line a (imaginary) particle that travels with the bulk velocity. The position of the characteristic points defined in § 3.1 are also shown so that we can compare the location of the particles with the position of these characteristic points of the puff and slug.

Only a cursory inspection of the figure reveals that the length of the histograms is much larger for the puff than for the slug. This can be attributed, as already seen in § 3.3, to the velocity profile in a puff being less 'well-mixed' than in a slug. This would clearly promote differential displacement of fluid particles that are initially randomly distributed over a cross-section. Moreover, the turbulence intensity in a slug has been found to be larger than in the puff. The mixing of particles would therefore be better in the slug than in the puff which results in the more uniform distribution of particles in the former structure.

Let us now consider the results for the particles released from planes II, III and IV, i.e. inside the puff/slug, in somewhat more detail. For the case of the puff, we see that of all particles released from plane IV an appreciable number can escape from the puff through the trailing edge. These are most likely to be the particles near the wall which due to the lower velocity there with respect to the propagation velocity of the puff are left behind. However, we also find that particles released from plane III and even from plane II are able to escape from the puff again through the trailing edge. On the other hand, none of the particles released from these three planes escape through the leading edge. In contrast, we find that for the slug almost all particles leaving planes II, III and IV stay within the slug and only very few particles (and only those leaving from plane IV) are able to escape through the trailing edge. These

https://doi.org/10.1017/S0022112099004681 Published online by Cambridge University Press

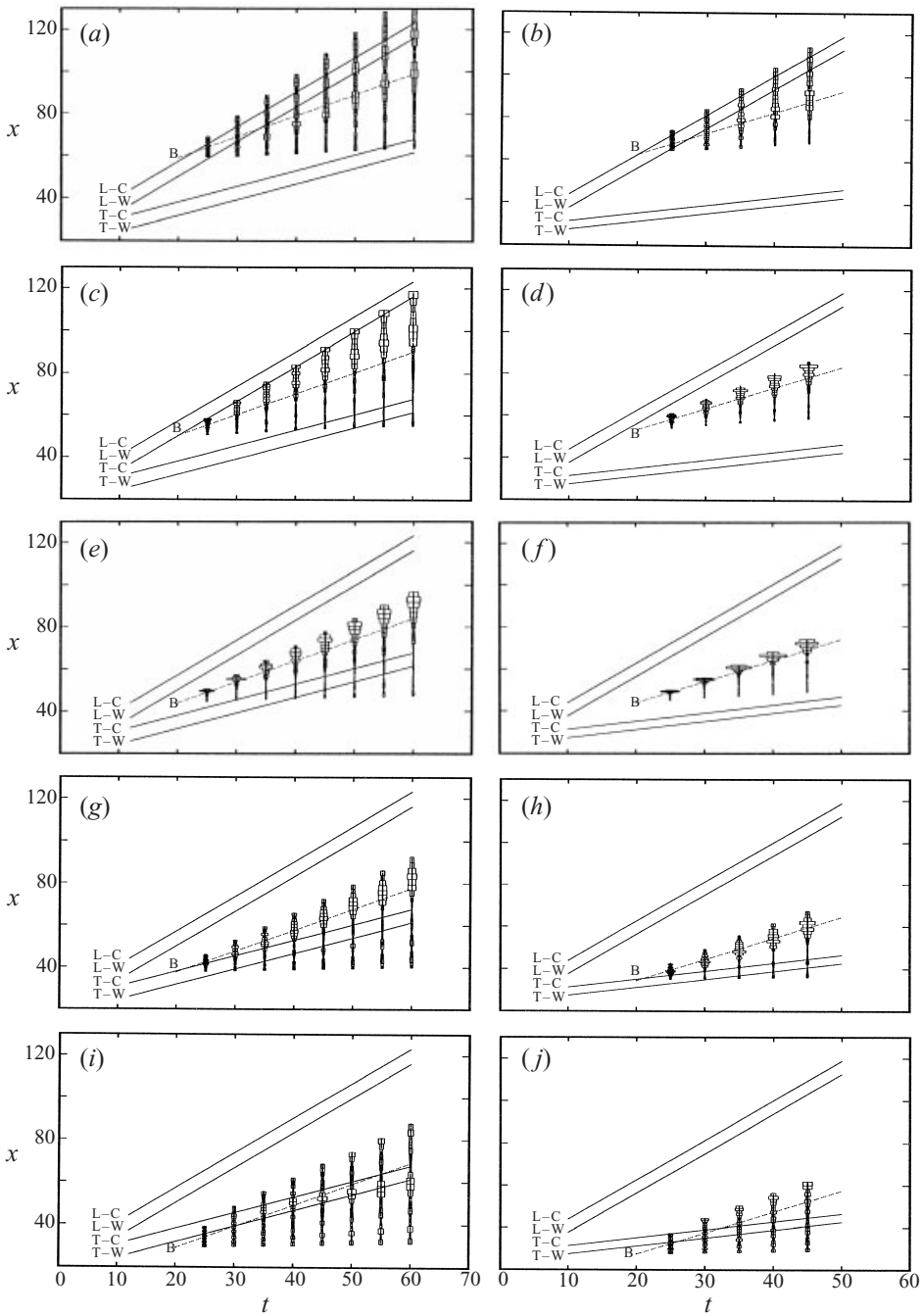


FIGURE 14. Statistics of particle trajectories released from planes I–V given in figure 4 for a puff and a slug. The positions of the particles at a given time are indicated by means of line histograms. The length of the line indicates the range in particle position and the width of the line gives the relative number of particles that have been found at that position. The dashed line, which starts at the initial position of the particle, shows the motion of a particle that travels with the bulk velocity U_B. In the figure we have also indicated the position of the characteristic points defined in § 3.1. (*a*) (*c*) (*e*) (*g*) (*i*) puff I, II, III, IV, V; (*b*) (*d*) (*f*) (*h*) (*j*) slug I, II, III, IV, V.

https://doi.org/10.1017/S0022112099004681 Published online by Cambridge University Press

results imply that a puff loses an appreciable amount of its material through the trailing edge whereas the slug is able to retain most of its material. This would explain the quicker growth of the slug with respect to the puff.

Next we consider the particles that leave from cross-section V that is initially behind the puff or slug. We see that for the case of the puff most of this material is left behind (especially at the later times) whereas for the slug most of the particles are entrained into the middle segment. For the particles that leave from plane I, which is initially in front of the puff or slug, we find that for both structures most eventually end up in either the puff or slug. These entrainment/detrainment characteristics are in agreement with the measurements of Wygnanski & Champagne (1973).

These results may be summarized as follows. A slug is entraining material both at its leading and trailing edge and a puff is entraining only at its leading edge. Moreover, a slug is able to retain most of its material whereas a puff is losing material or detraining across its trailing edge. This could perhaps be interpreted as that a slug has the characteristics of a material structure, i.e. containing all material that it entrains, whereas a puff behaves also as a wave-like structure, i.e. interchanging material with the surrounding fluid so that it is not always composed of the same fluid particles.

4. Details of the velocity field inside a puff

We have limited this investigation to the puff only because, as argued before, the resolution for the slug calculation may not be sufficient for a completely resolved computation of all flow details.

4.1. *Streamline pattern*

Let us consider the azimuthally and time-averaged streamline pattern on a meridian plane through the puff. To compute this pattern, we must solve the equation

$$\frac{\partial^2\psi}{\partial x^2}+\frac{\partial^2\psi}{\partial r^2}-\frac{1}{r}\frac{\partial\psi}{\partial r}=-r\omega_\theta, \tag{4.1}$$

where ψ is the streamfunction and ω_θ the ensemble-averaged azimuthal vorticity component. The streamfunction is related to the axial (v_x) and radial (v_r) components of the velocity by

$$v_x=\frac{1}{r}\frac{\partial\psi}{\partial r},\quad v_r=-\frac{1}{r}\frac{\partial\psi}{\partial x}. \tag{4.2}$$

Equation (4.1) is now solved subject to the boundary condition $\psi\,|_{r=0}=0$ and $\psi\,|_{r=1}=0$. This means that we consider the streamline pattern in a reference frame that travels with the mean velocity U_B. In that case at each cross-section the volume transport which is proportional to $\psi\,|_{r=0}-\psi\,|_{r=1}$, is equal to zero.

The resulting streamline pattern is shown in figure 15. Near the trailing-edge and leading-edge regions we observe recirculation patterns. These are consistent with the fact that, as we have already seen in § 3.3, the velocity distribution inside a puff or slug is more well-mixed than for the parabolic laminar profile. The recirculation pattern implies that in the frame moving with U_B at the leading edge fluid enters the puff/slug near the wall and leaves the puff/slug near the centreline. For the trailing edge the opposite occurs, i.e. fluid enters at the centreline and leaves near the wall region. However, we emphasize here that we have found in § 3.1 that the leading-edge and trailing edge of both the puff and slug do not travel with the bulk speed U_B.

https://doi.org/10.1017/S0022112099004681 Published online by Cambridge University Press

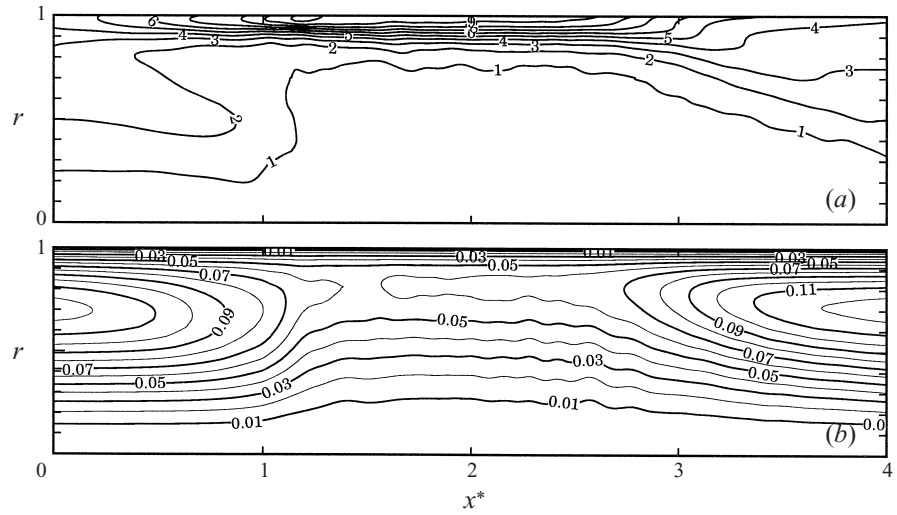


FIGURE 15. Ensemble-averaged pattern of the azimuthal vorticity component (*a*) and the streamlines (*b*) of a puff for a coordinate system that travels with the bull velocity U_B.

Therefore, one cannot interpreted the circulation patterns in terms of entrainment or detrainment of the puff/slug.

It is not difficult to recalculate the streamline patterns for a coordinate system that moves with either the trailing-edge or leading-edge velocity. The results are found to be comparable to the data which have been presented for such patterns by Wygnanski & Champagne (1973), Wygnanski *et al.* (1975) and Rubin, Wygnanski & Haritonidis (1980). Based on these results which also show recirculation patterns near the leading and trailing edge Wygnanski & Champagne (1973) propose the existence of toroidal vortices. However, such a vortex pattern has not been observed in our instantaneous velocity fields. Therefore, their existence is doubtful which agrees with the conclusion of Bandyopadhay (1986) based on flow visualizations. Nevertheless it is clear that these recirculation patterns are connected to the shape and dynamics of both the leading and trailing edge of the puff/slug.

4.2. *Helical motions*

Until now we have presented ensemble-averaged results, i.e. data which are averaged both in time and over the azimuthal direction. In this section we present some results of the instantaneous azimuthal variation of the velocity field.

In figure 16 we show a plot of the instantaneous streamwise vorticity in a cross-section near the leading edge and trailing edge of the puff at time $t = 32$. In these plots we can distinguish some circulation patterns which can be interpreted as a vortex pair. The vortex pairs are especially clear in the plot of the streamwise vorticity near the trailing edge where even several of these vortex pairs seem to be present. Similar streamwise vortex patterns have been also found near the trailing edge in the experimental results of Bandyopadhay (1986) and Eliahou, Tumin & Wygnanski (1998). A vortex pair, though rather weak, is also present in our results near the leading-edge cross-section. The combination of these vortex pairs with the general axial flow motion would imply that the particles are following helical trajectories in the flow.

All vortex pairs in figure 16 are found to be symmetric with respect to a vertical

https://doi.org/10.1017/S0022112099004681 Published online by Cambridge University Press

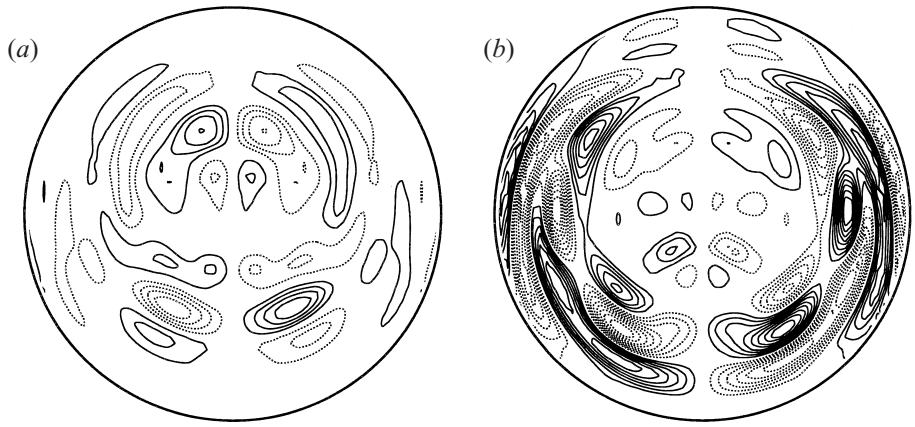


FIGURE 16. Isoline plot of the instantaneous streamwise vorticity in a plane near the leading edge (*a*) and trailing edge (*b*) of the puff at $t = 32$. Contour spacing 0.1, dotted line negative.

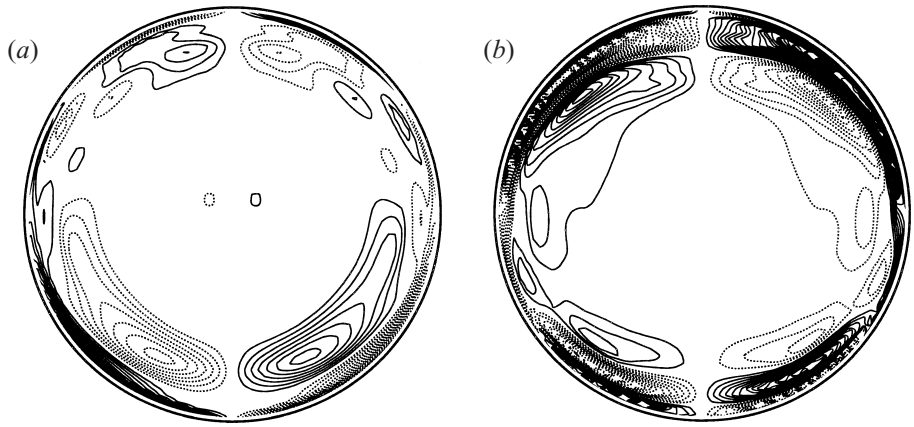


FIGURE 17. Isoline plot of the instantaneous streamwise vorticity in a plane near the leading edge (*a*) and trailing edge (*b*) of the puff at $t = 2.6$ when the introduced disturbance had just stopped. Contour spacing 0.1, dotted line negative.

line through the pipe axis. From this symmetry property we deduce that they are related to the initial perturbation (2.9) which is also symmetric with respect to the same axis. This observation is confirmed in figure 17 where we show plots of the streamwise vorticity near the leading edge and trailing edge of the puff just after the perturbation has stopped. The existence of the streamwise vortices is very clear and they seem to concentrate near the wall.

The streamwise vortices which we have found here are believed to play an essential role in the turbulence generating mechanism proposed by Waleffe (1997) which is called a self-sustained process. In this mechanism a pair streamwise vortices cause inflection points in the axial velocity which subsequently becomes unstable. The resulting instability process is called a burst and it is able to regenerate the streamwise vortices so that a next cycle can develop. We note, that apart from the streamwise vortices, we have observed in our simulation results another ingredient of the self-sustained process, namely the appearance of inflection points in the axial velocity profiles shown in figure 6. The appearance of both streamwise vortices and inflection

https://doi.org/10.1017/S0022112099004681 Published online by Cambridge University Press

points in our simulation results should in our opinion be considered as significant and their role should be studied further.

5. Conclusions

In this study we have performed a numerical simulation of a puff and a slug structure in a transitional pipe flow at a Reynolds number of $Re = 2200$ and $Re = 5000$, respectively. The simulation has been carried out with a spectral element method which combines a high accuracy with an adequate resolution in the different regions of the pipe. Based on the results of the computations we can draw the following conclusions.

(*a*) The leading edge and trailing edge of both a puff and a slug travel with a constant velocity which we found to be in reasonable agreement with experimental data. The propagation velocity of the total puff and slug structure is approximately equal to the bulk velocity.

(*b*) With help of a procedure to compute ensemble averages, we have determined several aspects of the mean structure of a puff and a slug. First the velocity profile confirms the behaviour found in experiments that near the leading edge the centreline velocity of a puff varies more gradually than in the case of a slug. The wall shear stress and the velocity fluctuations showed a plateau region in the middle segment for the case of the puff and a double maximum near both the trailing and leading edge for the case of the slug. Furthermore, we found that the turbulence within the slug is quite close to the structure of a fully developed turbulent pipe flow. This result agrees with experimental observations.

(*c*) With help of computations for various values of the initial condition we could estimate that the influence of the details of the initial disturbance on the further development of the puff and slug is small. This would imply that the influence of the initial disturbance can be neglected which was also found in experiments. Furthermore, we have also performed computations for a puff at various values of the Reynolds number below 2200 and found that the growth of the disturbance energy decreases as the Reynolds number becomes smaller. It also seems that below the value $Re = 2200$ the disturbance energy decays after having reached a maximum value.

(*d*) By computing the trajectories of fluid particles released from several cross-sections within and outside the puff/slug structure, we determined the following characteristics of both structures. The slug entrains material at both the leading and trailing edge and keeps the material which it entrains inside it. Together with the fact that the slug seems to travel at a speed close to the bulk velocity we venture to conclude that a slug is a material property of the flow. On the other hand, the puff entrains material only through its leading edge and detrains material across its trailing edge. This means that the puff constantly exchanges material with the laminar flow outside the puff. Based on these facts we would characterize the puff to be more wave-like.

(*e*) For the case of the puff we have computed several further details of the flow field. The ensemble-averaged streamline pattern was computed in a frame that travels with the bulk velocity. This streamline pattern showed recirculation patterns in the leading-edge and trailing-edge regions which have been also observed in experiments. Moreover, based on isoline plots of streamwise vorticity we conclude that helical particle motions exist in the trailing-edge region. Such motions have been also observed in experiments and they are believed to play a role in the transition process.

https://doi.org/10.1017/S0022112099004681 Published online by Cambridge University Press

The first author expresses gratitude to the Delft University of Technology for financial support for one year to carry out this study. The second and third authors are indebted to the Delft University of Technology for financial support during this project. The fourth author is indebted to Tsinghua University for financial support for a visit during which this article was written. The third author is also grateful to the National Natural Science Foundation of China (NNSFC) for the support of the project. All authors are grateful to Drs M. Hulsen and L. Timmermans for discussions related to the numerical techniques and to Professor I. Wygnanski for his comments on the first draft of this paper.

REFERENCES

Bandyopadhay, P. R. 1986 Aspects of the equilibrium puff in transitional pipe flow. *J. Fluid Mech.* **163**, 439–458.

Darbyshire, A. G. & Mullin, T. 1995 Transition to turbulence in constant-mass-flux pipe flow. *J. Fluid Mech.* **289**, 83–114.

Draad, A. A. 1996 Laminar-turbulent transition in pipe flow for Newtonian and non-Newtonian fluids. PhD thesis, Delft University of Technology, the Netherlands.

Draad A. A. & Westerweel, J. 1996 Measurement of temporal and spatial evolution of transitional pipe flow with PIV. Presentation at the Meeting of the APS, Fluid Mechanics Section, University of Buffalo, NY.

Eggels, J. G. M., Unger, F., Weiss, M. H., Westerweel, J., Adrian, R. J., Friedrich, R. & Nieuwstadt, F. T. M. 1994 Fully developed pipe flow: a comparison between direct numerical simulation and experiment *J. Fluid Mech.* **268**, 175–209.

Eliahou, S., Tumin, A. & Wygnanski, I. 1998 Laminar-turbulent transition in Poiseuille pipe flow subjected to periodic perturbation emanating from the wall. *J. Fluid Mech.* **361**, 333–349.

Gottlieb, D., Hussaini, M. Y. & Orszag, S. A. 1984 Theory and applications of spectral methods. In *Spectral Methods for Partial Differential Equations* (ed. R. G. Voigt, D. Gottlieb & M. Y. Hussaini), pp. 1–54. SIAM.

Karniadakis, G. E., Israeli, M. & Orszag, S. A. 1991 High-order splitting methods for the incompressible Navier–Stokes equations. *J. Comput. Phys.* **97**, 414–443.

Kleiser, L. & Zang, T. A. 1991 Numerical simulation of transition in wall-bounded shear flows *Ann. Rev. Fluid Mech.* **23**, 495–537.

Marcus, P. S. 1984 Simulation of Taylor–Couette flow. Part 1. numerical methods and comparison with experiment. *J. Fluid Mech.* **146**, 45–64.

Orszag, S. A. & Patera, A. T. 1983 Secondary instability of wall-bounded shear flows. *J. Fluid Mech.* **128**, 347–385.

O'Sullivan, P. L. & Breuer, K. S. 1994*a* Transient growth in circular pipe flow. I. Linear disturbances. *Phys. Fluids* **6**, 3643–3651.

O'Sullivan, P. L. & Breuer, K. S. 1994*b* Transient growth in circular pipe flow. II. Nonlinear development. *Phys. Fluids* **6**, 3652–3665.

Reynolds, O. 1883 An experimental investigation of the circumstance which determine whether the motion of water shell be direct or sinuous, and the law of resistance in parallel channel. *Phil. Trans. R. Soc. Lond.* A **186**, 835–982.

Rubin, Y., Wygnanski, I. J. & Haritonidis, J. H. 1980 Further observations on the transition in a pipe. In *Laminar-Turbulent Transition, IUTAM Symposium Stuttgart, Germany 1979*, pp. 17–26. Springer.

Teitgen, R. 1980 Laminar-turbulent transition in pipe flow: development and structure of the turbulent slug. In *Laminar-Turbulent Transition, IUTAM Symposium Stuttgart, Germany 1979*, pp. 27–36. Springer.

Waleffe, F. 1997 On a self-sustaining process in shear flows. *Phys. Fluids* **7**, 883–900.

Wygnanski, I. J. & Champagne, F. H. 1973 On transition in a pipe. Part 1. The origin of puffs and slugs and the flow in a turbulent slug. *J. Fluid Mech.* **59**, 281–335.

Wygnanski, I. J., Sokolov, M. & Friedman, D. 1975 On transition in a pipe. Part 2. The equilibrium puff. *J. Fluid Mech.* **69**, 283–304.

https://doi.org/10.1017/S0022112099004681 Published online by Cambridge University Press